 

PACS numbers: 42.79.Qx; 92.20.Ny
DOI: 10.1070/QE2001v031n08ABEH002038

# Shore-based lidar for monitoring coastal sea water areas

S A Burikov, D V Klimov, P N Litvinov, D V Maslov, V V Fadeev

*Abstract*. **A shore-based lidar, which plays a vital role in the creation of continuous express monitoring of coastal sea water areas, is described. The results of testing in the region of the Blue Bay (Black Sea, near Gelendzhik) are reported. Echo-signal spectra were recorded by exciting water by light at wavelengths 532, 355 and 266 nm (second, third and fourth harmonics of a Nd:YAG laser). The dependence of the echo signal (Raman scattering of light by water molecules) on the sensing range is studied. The obtained results are in good agreement with the theory of remote laser sensing developed in this work for large sensing angles, in which the wind waves play a key role. A sensing range of 100 m was achieved using 532-nm, 10-ns laser pulses at a pulse repetition rate of 10 Hz and the pulse energy of 10 mJ. The possibility of increasing the sensing range to 0.5 – 1 km is shown.**

***Keywords***: *shore-based lidar, coastal water region, wind waves, remote sensing, echo signal, Raman scattering, fluorescence.*

## 1. Introduction

Investigations of the methods and tools of laser monitoring of aqueous media, which are being carried out during the last quarter of the century by many research teams all over the world, have revealed unique potentialities of lasers (see, for example, Refs. [1 – 4]). Apparently, it is high time to utilise these measuring complexes to solve specific problems concerning the monitoring of particular water areas. Among such areas, coastal waters (especially sea water areas), waterways near ports, recreation areas, oil-loading terminals and water reservoirs, etc. occupy a special position.

The concept of such a monitoring in which the main element of the system is a lidar mounted on a sufficiently high building on the shore was developed in Ref. [5]. The lidar carries out continuous (or quasi-continuos) monitoring of the water surface and surface layers (and, possibly, the atmospheric layer near the water surface) in the chosen water area. The efficiency/cost ratio for continuous monitoring of coastal water areas with the help of such a lidar is much higher than for other methods (like sampling, probing from an aircraft or a ship).

It was shown in Refs [1, 6, 7] that the sensing range of a lidar detecting Raman signal of water (and fluorescence signals of comparable intensities from organic impurities) may be as long as several kilometres (for normal incidence of the laser beam on the surface of water). However, the possibility of lidar probing of the coastal water areas requires a special analysis because the sensing range $R$ and the sensing angle $\theta$ may vary over broad intervals, the angle $\theta$ attaining values close to 90° as the range $R$ increases to the required values $\sim 0.5 - 1$ km [the sensing angle $\theta$ is the angle between the laser beam and the normal to the water surface under the assumption that the latter is a horizontal plane (Fig. 1)]. For example, during the scanning of the Blue Bay in the Black Sea using the lidar devised by us and mounted at a height of 10 m over the sea surface, the sensing angle varies from 78.6 to 88.9° as the sensing range varies from 50 to 500 m. In this case, difficulties are encountered in echo-signal recording due to an increase in the distance $R$ and 'Fresnel' losses related to the reflection of light from the water surface. Moreover, the surface of the sea is not perfectly smooth (flat), so that the local angle of incidence $\varphi$ (the angle between the normal to an element of water surface and the laser beam) may differ significantly from 90°, thus enhancing the intensity of the detected echo signal. Thus, while analysing the possibility of probing of coastal sea water areas by a shore-based lidar, the wind waves should be taken into account, which concerns a spectroscopic lidar used for monitoring with the help of fluorimetric and Raman scattering methods.

## 2. Echo signal and peculiarities of its formation during sensing by a shore-based lidar (theory)

### 2.1 Wind waves model

To study the peculiarities of formation of an echo signal during laser sensing of the sea waters through a wavy sur-

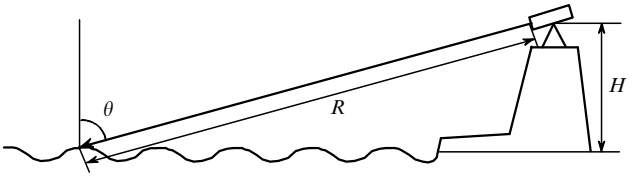


**Figure 1.** Schematic diagram for remote sensing of coastal sea water area with a shore-based lidar.

**S A Burikov, D V Klimov, P N Litvinov, D V Maslov, V V Fadeev**
Department of Physics, M V Lomonosov Moscow State University, Vorob'evy gory, 119899 Moscow, Russia

Received 1 March 2001
*Kvantovaya Elektronika* **31** (8) 745 – 750 (2001)
Translated by Ram Wadhwa

face (for large values of $\theta$), we used the model concepts about wavy surfaces described in Ref. [8]. Out of the two possible approaches to the description of random wind waves, the statistical approach and the spectral approach, we chose the first approach, which allows us to characterise the waves in terms of the mean values and the distribution functions of the parameters of wave elements present at the sea surface.

Waving of the sea is a nonuniform and nonstationary random process. For the purpose of analysis, however, this process can be assumed stationary and quasi-uniform within certain space and time intervals, and also ergodic. Let the ruffled surface be characterised by a random function of time $z(x, y, t)$, where $z$ is the ordinate of the surface over the unperturbed water level, and $x$ and $y$ are the horizontal displacements of a point on the water surface along the corresponding axes. It was shown in Ref. [8] that, under the assumptions made above, the ordinate $z$ of the wavy surface obeys the one-dimensional normal distribution law

$$g(z) = \frac{1}{(2\pi\delta^2)^{1/2}} \exp\left[-\frac{(z-\bar{z})^2}{2\delta^2}\right], \tag{1}$$

where $\bar{z} = 0$; and $\delta^2$ is the variance of the ordinates of the surface.

Similar distribution functions $g(x)$ and $g(y)$ are valid for the horizontal displacements $x$ and $y$ of water particles. In this case, the distribution function for the slopes of the ruffled surface elements satisfies in the first approximation the two-dimensional normal law:

$$f(z_x, z_y) = \frac{1}{2\pi\sigma^2} \exp\left(-\frac{z_x^2 + z_y^2}{2\sigma^2}\right), \quad z_x, z_y \in [-\infty;\ +\infty], \tag{2}$$

where $z_x, z_y$ are the slopes of the surface defined in the form $z(x, y, t)$ in the planes $zx$ and $zy$, respectively; and $\sigma$ is the standard deviation for which the distribution function decreases by a factor of $e^{-1/2} = 0.6$ relative to its maximum. It is convenient to characterise the sea waves with the help of the parameter $d$, the characteristic wave angle (usually measured in degrees) satisfying the relation $d = \sigma$.

The asymmetry of the wave slopes in the direction of the wind (the leeward slope is steeper than the windward slope) leads to an asymmetry of the distribution curve. In this case, the distribution function is best described by a Gram–Charlier series [8].

### 2.2 Echo-signal formation model. The return factor

The following assumptions were made while constructing the model of echo-signal formation during water surface probing taking into account the wind wave statistics:

(1) the distribution of the surface elevation is normal;

(2) the variances of the distribution of slopes of the waved surface elements along the $x$- and $y$-axes are identical, i.e., the wind direction is disregarded;

(3) the probing laser beam cross section diameter is either larger than the characteristic length of the sea waves or averaging is carried out by signal accumulation;

(4) if the local angle of beam incidence on the water surface element exceeds 90°, the beam does not contribute to the echo signal; i.e., we do not consider the partial transmission of the laser beam through a wave followed by its participation in the signal formation;

(5) the propagation of the beams follows the geometrical optics approximation;

(6) the dispersion of the refractive index of water (relative to air) in the region of wavelengths of the exciting radiation and the echo signal is neglected.

To find the angle $\varphi$ of incidence of the sensing laser beam on the surface element $z(x, y, t)$, we introduce a unit vector $\boldsymbol{k}$ along the probing direction and the vector $\boldsymbol{n}$ normal to the surface. Assuming that vector $\boldsymbol{k}$ and the unit electric field vector $\boldsymbol{e}$ lie in the plane $zx$, we obtain

$$\boldsymbol{k} = \{\sin\theta, 0, -\cos\theta\}, \quad \boldsymbol{e} = \{\cos\theta, 0, \sin\theta\}.$$

By choosing the vector normal to the surface in such a way that its ordinate is equal to unity, we obtain $\boldsymbol{n} = \{-z_x, -z_y, 1\}$ and, consequently, $n = (z_x^2 + z_y^2 + 1)^{1/2}$. The angle $\varphi$ between vectors $\boldsymbol{n}$ and $\boldsymbol{k}$ is defined by the formula

$$\cos\varphi(z_x, z_y) = \frac{\boldsymbol{nk}}{nk} = \frac{-\cos\theta - z_x \sin\theta}{(z_x^2 + z_y^2 + 1)^{1/2}}. \tag{3}$$

We define the return factor $K(\varphi)$ as the product of the coefficients of transmission of the exciting (laser) radiation ($K_1$) and of the echo signal ($K_2$) (Raman scattering of light by water molecules, impurity fluorescence, etc.) through a local element of the water surface:

$$K(\varphi) = K_1 K_2. \tag{4}$$

Thus, we have two random quantities $z_x$ and $z_y$ with the distribution function (2), angle $\varphi$ as a function of these quantities, and the transmission coefficients $K_1$ and $K_2$ as functions of $\varphi$. In this case, the recovery coefficient averaged over the distribution of incidence angles has the form

$$\bar{K} = \int_{-\infty}^{+\infty} \int_{-\infty}^{+\infty} K(\varphi(z_x, z_y)) D[\cos\varphi(z_x, z_y)] \times f(z_x, z_y)\,\mathrm{d}z_x\mathrm{d}z_y, \tag{5}$$

where

$$D(\alpha) = \begin{cases} 1, & \alpha \geqslant 0, \\ 0, & \alpha < 0. \end{cases}$$

The factor $D(\alpha)$ owes its origin to the assumption 4 made above, and nullifies the integrand for the ruffled surface elements on which the beam incidence angle exceeds 90°. It can be shown that as $d \to 0$ and the ruffled surface is transformed into a plane, the coefficient $\bar{K}$ tends to the return factor for a plane.

The complexity of the form of Fresnel coefficients does not allow us to obtain an analytic expression for integral (5). For this reason, we calculated $\bar{K}$ numerically for two cases (one-dimensional and two-dimensional) of the sea surface ruffling.

In the one-dimensional case ($z_x \neq 0, z_y = 0$), the exciting radiation is linearly polarised in the incidence plane, and hence $K_1 = K_p$ ($K_p$ and $K_s$ are the Fresnel transmission coefficients for p- and s-polarised light, respectively). As a rule, the echo signal (due to fluorescence or some kind of scattering) is partially depolarised, so that $K_2$ is defined by the expression

$$K_2 = A_2 K_p + B_2 K_s, \quad A_2 + B_2 = 1. \tag{6}$$

Coefficients $A_2$ and $B_2$ characterise the degree of depolarisation of the echo signal and can be represented in terms of the depolarisation factor $\rho = I_\perp / I_{||}$, which is equal to the ratio of the intensities of depolarised ($I_\perp$) and non-depolarised ($I_{||}$) components of the echo signal:

$$A_2 = \frac{1}{1+\rho}, \quad B_2 = \frac{\rho}{1+\rho}. \tag{7}$$

In the case under study, when the echo signal is a signal of Raman scattering of light by water molecules, $\rho = 0.18$ [9]. Thus, in the case of one-dimensional waving, the return factor is defined as

$$K(\varphi) = K_\mathrm{p}(A_2 K_\mathrm{p} + B_2 K_\mathrm{s}). \tag{8}$$

The solid curves in Fig. 2 show the dependences of the mean recovery coefficient $\bar{K}$ on the sensing angle $\theta$ calculated from expression (5) taking formulas (7) and (8) into account. One can see that in the case of an intense waving for sensing angles close to 90°, the return factor is smaller than for normal incidence by a factor of 2–3 only. The curves $\bar{K}(\theta)$ intersect at a single point with coordinates 82°, 0.46 with an error of 4 % and 7 % along the abscissa and the ordinate axes, respectively. Thus, angle $\theta \approx 82^\circ$ corresponding to the intersection of the curves is the boundary between the two cases of sensing: the strongest echo signal for $\theta < 82^\circ$ is detected in the absence of wind waves, while the strongest echo signal for $\theta > 82^\circ$ is detected in the presence of wind waves.

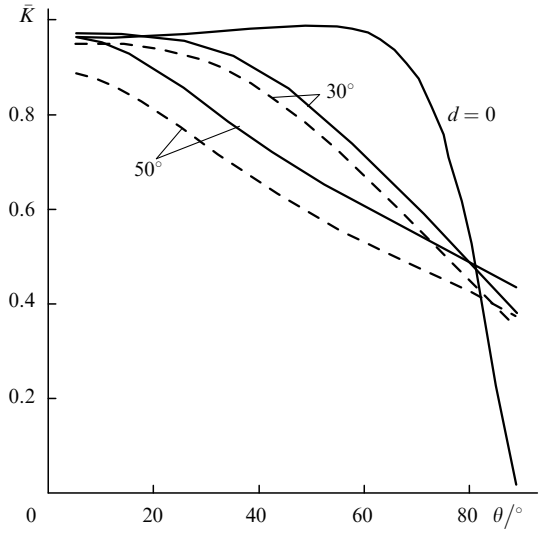


**Figure 2.** Dependences of the mean return factor on the sensing angle $\theta$ for the cases when the exciting radiation is polarised in the $zx$ plane, and the distribution of the wave slopes is one-dimensional (in the $zx$ plane, solid curves) or two-dimensional (dashed curves) for various angles $d$ and echo signal depolarisation factor $\rho = 0.18$.

Calculations up to this level were earlier carried out by our group for the case when the echo signal is a fluorescence signal (depolarisation factor $\rho = 1$). The results of these calculations were reported at the conference in Seattle and were published in its proceedings [10]. It was shown that a change in the parameter $\rho$ from 1 to 0.18 changes the dependence $\bar{K}(\theta)$ by no more than 10 %. In view of the planned field testing of the theory, we will consider here the two-dimensional waves on the sea surface ($z_x \neq 0$, $z_y \neq 0$), which are closer to the real experimental conditions.

In this case, the vector $\boldsymbol{n}\left(\varphi(z_x, z_y)\right)$ characterising the local area element does not lie in the $zx$ plane. Therefore, the plane of beam incidence on the local area element of the water surface formed by vectors $\boldsymbol{n}$ and $\boldsymbol{k}$ (it is assumed that the vectors $\boldsymbol{k}$ and $\boldsymbol{e}$ lie in the $zx$ plane as before) does not coincide with the $zx$ plane, and the vector $\boldsymbol{e}$ forms a certain angle $\psi(z_x, z_y)$ with the normal to the plane of incidence on the local area element. This angle can be expressed in terms of the quantities $z_x, z_y$ and $\theta$, which leads to an analytic expression similar to (8) for the coefficient $K(\varphi)$. Using this expression, the dependences $\bar{K}(\theta)$ were calculated with the help of formula (5). Fig. 2 shows examples of such dependences (dashed curves) which are compared with the dependences $\bar{K}(\theta)$ calculated for one-dimensional waving (solid curves). One can see from this comparison that a consideration the two-dimensional distribution of the slopes does not affect the curves $\bar{K}(\theta)$ significantly.

Thus, the wind wave model used by us leads to the following important conclusion: for sensing angles close to 90°, the received echo signal will be weaker than the signal obtained for normal incidence on the water surface by a factor of 2–3 only. Hence, it is possible, in principle, to carry out probing at angles close to 90°.

### 2.3 Calculations of the echo-signal dependence on the sensing range

The problem about the influence of the echo signal caused by inelastic scattering of laser radiation in water (fluorescence, Raman scattering) was solved in Refs [6, 11] for the general case using the radiation transport equation in the small-angle approximation. We shall confine our analysis to a simpler case of the Bouguer approximation, which leads to the following expression for the number $N_2$ of echo signal photons incident on the aperture of the lidar detector:

$$N_2 = \sigma^\pi n N_1 A\Omega\, \bar{K}(\theta) \int_0^\infty \mathrm{d}l \exp\left[-(\varepsilon_{650} + \varepsilon_{532})l\right], \tag{9}$$

where $\sigma^\pi$ is the differential cross section for transformation of the probing radiation into an echo signal in the direction $\pi$ (in the case of our experiments, this cross section corresponds to Raman scattering in water or to the fluorescence of chlorophyll a in phytoplankton); $n$ is the concentration of water molecules or the fluorescent impurity; $N_1$ is the number of probing radiation photons (it is assumed that the probing radiation is transformed linearly into the echo signal, e.g., in the absence of fluorescence saturation); $l$ is the coordinate along the beam in water ($l = 0$ corresponds to the water surface); $\Delta\Omega = (A/R)^2$ is the solid angle of the detector; $A$ is the detector aperture; $R \gg l_0$ is the sensing range, which is assumed to be equal to the distance between the lidar and the wave surface; $l_0$ is the length of the water layer making the dominant (say, up to 95 %) contribution to the echo signal; and $\varepsilon_{650}, \varepsilon_{532}$ are the light attenuation coefficients in water at the wavelengths of the probing radiation and the echo signal, respectively.

It follows from (9) that under the conditions of constant attenuation coefficients in the surface layer and a constant probing geometry, the ratio of the echo signals for two detection ranges $R$ and $R_0$ will be determined by the expression

$$\frac{N_2(R)}{N_2(R_0)} = \left(\frac{R_0}{R}\right)^2 \frac{\bar{K}\big(\theta(R)\big)}{\bar{K}\big(\theta(R_0)\big)}. \qquad (10)$$

It follows from this expression that if no waves are formed as $R$ increases and $\theta$ approaches 90°, the echo signal being detected will decrease more rapidly than $R^{-2}$ due to a sharp decrease in the value of $\bar{K}$ as $\theta$ approaches 90° (Fig. 2, $d = 0$). However, in the case of intense ruffling ($d \geqslant 30$°), the coefficient $\bar{K}$ does not change by more than 10 % upon a variation of $\theta$ from 70 to 90° (see Fig. 2), and hence the dependence of the echo signal on $R$ will be close to $R^{-2}$, as in the case of normal incidence of the exciting radiation on the water surface. This is illustrated in Fig. 3 showing the dependences $N_2(R) = N_{RS}(R)$ calculated for the Raman scattering signal in water excited at 532 nm; the wavelength of the Raman band maximum being 650 nm.

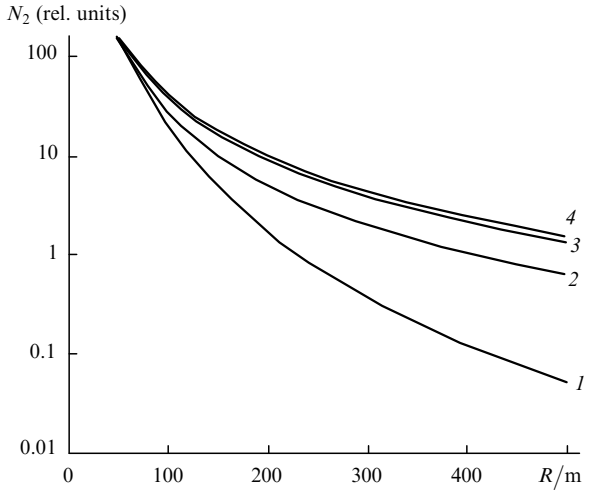


**Figure 3.** Theoretical dependences of the echo signal $N_2$ (Raman band of water) on the sensing range $R$, normalised to the signal at $R = 50$ m, for the case of incidence on a flat surface (curve *1*), incidence on a waved surface for $d = 10$ (curve *2*) and 50° (curve *3*), and for the case of normal incidence (curve *4*). The height $H$ of the lidar over the sea surface is ~ 10 m, the exciting radiation is $p$-polarised, and the depolarisation factor of the echo signal is $\rho = 0.18$.

## 3. Experiment

The experimental results were obtained in the course of an expedition organised in September 2000 in the Blue Bay (Black Sea, near Gelendzhik). The lidar was mounted on the third floor of a building on the sea shore, so that the height of the lidar above the sea level was 10 m (see Fig. 1). The probing angle was varied from 78 to 83°, which corresponds to a sensing range between 50 and 80 m. A special test (see below) showed that the power characteristics of the lidar made it possible to increase the sensing range to 150 – 200 m, although these potentialities could not be realised in actual practice due to flaws in the construction of the lidar which was essentially a laboratory model.

### 3.1 Technical characteristics of the lidar

The laser radiation source in the lidar was a two-stage Nd:YAG laser with frequency conversion. The 532-nm second harmonic of the laser radiation was used for adjusting the lidar (relative to the Raman band of water) and for studying the dependence of the echo signal on the sensing range. The possibility of monitoring the temperature, salinity and organic impurity characteristics by using the second, third ($\lambda = 355$ nm) and fourth ($\lambda = 266$ nm) harmonics of laser radiation was also investigated. Table 1 shows the laser characteristics for these three wavelengths.

Signals were detected with an optical multichannel analyser (OMA) based on a 'DeltaTec' CCD array (Moscow State University Science Park), a Pentium II computer, and an EG&G polychromator (model 1226). The radiation was focused on the OMA slit with a lens of diameter 15 cm and focal length 50 cm. A quasi-coaxial system was used for probing. The distance between the axes of the laser and the receiver (base) at the lidar outlet was 20 cm. The lens focused the radiation incident on it to the OMA slit of width 0.5 mm and height 1 cm. For recording the spectra, the signal was accumulated over a period of 1 min. To improve the signal-to-noise ratio during daytime, the OMA operated in the sampling mode. The sensitivity range of the OMA was 250 – 900 nm, which permitted a recording of emission spectra upon excitation at all three lidar wavelengths.

**Table 1.** Parameter of laser radiation at the lidar output.

| Wavelength/nm | Pulse energy/mJ | Average power/mW | Divergence /mrad | Pulse repetition rate/Hz |
|---|---|---|---|---|
| 532 | 80 | 800 | 3 | 10 |
| 355 | 30 | 300 | 3 | 10 |
| 266 | 20 | 200 | 3 | 10 |

### 3.2 Dependence of the echo signal on the sensing distance

Fig. 4 shows a typical echo-signal spectrum obtained upon remote sensing by a lidar with a laser radiation wavelength of 532 nm. This spectrum contains the Raman band of water and the phytoplankton fluorescence bands. The Mie scattering line at the unshifted wavelength 532 nm was suppressed by a filter. The echo-signal spectra were also obtained by probing at two other wavelengths (355 and 266 nm). The structure of these spectra (as well as the structure of the spectrum obtained by probing at 532 nm) corresponds to that described in the literature (see, for example, Refs [1 – 3]).

The dependence of the echo signal on the sensing range was studied by using the Raman band of water because its intensity depends linearly on the intensity of the exciting signal over a large range of variation of the latter, and does not depend on the impurity concentration in water (or depends very weakly, e.g., on salinity). The procedure of spectral analysis included smoothing of the spectrum, interpolation of the background (whose origin was not investigated) to the region of the Raman band of water and the phytoplankton fluorescence band (600 – 750 nm) and the separation of these overlapped bands. Fig. 5 shows the experimental dependence of the echo signal (Raman band of water) on the sensing range. The figure also shows the theoretical dependences of the echo signal on the sensing range (normalised to the signal for $R = 50$ m) for various values of $d$ obtained from formula (10).

One can see from Fig. 5 that, upon an increase in the sensing range $R$, the echo signal does not decrease as rapidly as in the case of incidence on a smooth surface. The experimental points fall quite accurately on the theoretically calculated dependence of the echo signal on $R$ for $d = 50$°.

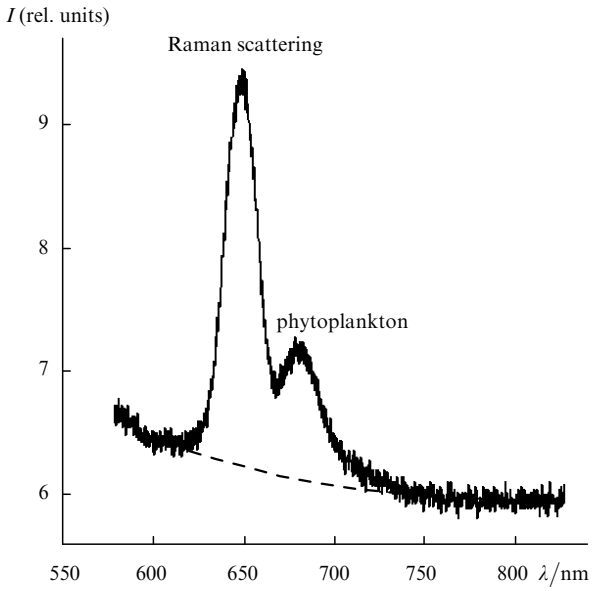


**Figure 4.** A typical echo signal spectrum obtained for remote sensing of the water surface in the Blue Bay by a shore-based lidar (excitation wavelength $\lambda = 532$ nm). The Raman band of water and the phytoplankton fluorescence band are shown.

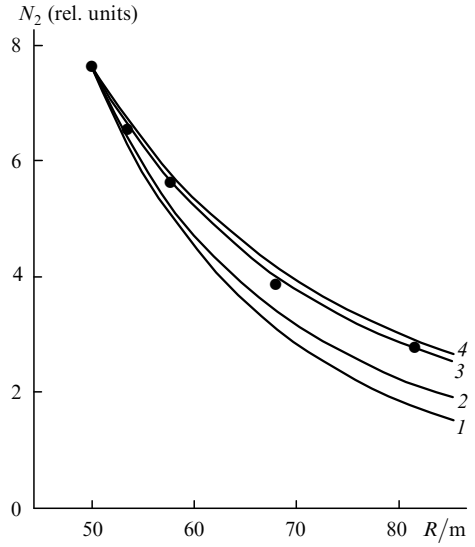


**Figure 5.** Experimental (points) and theoretical (curves) dependences of the echo signal $N_2$ (Raman scattering in water) on the sensing range for the laser wavelength $\lambda = 532$ nm. Calculations were made for incidence on a flat (plane) surface (curve *1*), incidence on a waved surface for $d =$ 10 (curve *2*) and 50° (curve *3*), and for the case of normal incidence (curve *4*). The height $H$ of the lidar over the sea surface is $\sim 10$ m. The theoretical curves are normalised to the signal at $R = 50$ m. The experimental point for $R = 50$ m corresponds to 154 counts on the photodetector.

This dependence virtually coincides with the dependence $R^{-2}$ corresponding to normal incidence.

It was mentioned above that the lidar in our experiments did not operate at its highest sensitivity. By increasing the signal accumulation time to 2 min, we could detect the Raman band of water at a distance of 50 m by reducing the pulse energy from 80 to 10 mJ, which corresponds to the average power of 100 MW for a pulse repetition rate of 10 Hz. Taking into account that the theoretical and experimental dependence of the echo signal on the sensing range is close to $R^{-2}$, we can predict that an increase in the average power to 10 W will allow us to increase the sensing range of a shore-based lidar up to 0.5 km. Using the potentialities of the detecting system and the lidar probing geometry (coaxial geometry, a large input aperture of the receiver and a higher sensitivity of the detector) the sensing range can apparently be increased to $\sim 1$ km, which corresponds to the characteristic range of coastal sea waters requiring continuous monitoring (waterways near ports, recreation areas, oil-loading terminals, etc.).

## 4. Conclusions

The results presented in this work reveal the possibility of creating a shore-based lidar for monitoring the coastal water areas for distances up to 1 km. For such a sensing range, the incidence angle on the water surface would be close to 90° for a smooth (flat) surface. The sharp increase in the Fresnel reflection would make the echo signal too weak for detection. This drawback is eliminated mainly due to the presence of wind waves: the echo signal for the probing angle $\theta \approx 90°$ is only about 2–3 times smaller than in the case of normal incidence.

The above conclusions of the theory were confirmed by testing of the laboratory sample of the lidar fabricated by us in the Black Sea (Blue Bay). Such a lidar, which can be used for probing at three different wavelengths (532, 355, and 266 nm) is capable of checking the temperature and salinity of water, phytoplankton parameters, parameters of organic impurities like aqueous humic substance and protein compounds, and oil contaminations in the form of films on the water surface, oil emulsions, as well as solutions in the bulk of water. Our group is engaged in a continuous quest for developing and perfecting the methodical approach and algorithms for solving the inverse problems as applied to the lidar [3, 5, 12–14].

***Acknowledgements.*** This work was supported by the Federal Special-Purpose Programme 'World Ocean' (Project No. 6.10) and the Federal Special-Purpose Programme 'Integration' (Project No. 475).

## References

1. Measures R *Laser Remote Sensing, Fundamentals and Applications* (New York: Wiley, 1984; Moscow: Mir, 1987)
2. Bravo-Zhivotovskii D M, Dolin L S, Savel'ev V A, et al. *Distantsionnye metody issledovaniya okeana* (Remote Methods For Ocean Studies) (Gor'kii, Inst. Appl.. Phys., Russian Academy of Sciences, 1987)
3. Fadeev V V, in *Proc. IV Intern. Conf. on Laser Applications in Life Sciences* (Jyväskylä, Finland, 1992, p. 410)
4. Gol'din Yu A, Luchinin A G, in *Poverkhnostnyi sloi okeana. Fizicheskie protsessy i distantsionnoe zondirovanie* (Surface Ocean Layer. Physical Processes and Remote Sensing) (Gor'kii, Inst. Appl. Phys., Russian Academy of Sciences, 1987)
5. Fadeev V V, Kompitsas M, Reuter R *Proc. Intern. Symp. 'Envirosense'* (Munich, Germany, 1999, p. 358)
6. Demidov A A, Klyshko D N, Fadeev V V *Vestn. Mosk. Univ., Ser. III* **19** No. 4 64 (1978)
7. Bartsch B, Braeske T, Reuter R *Appl. Opt.* **32** 6732 (1993)
8. Kononkova G E, Pokazeev KV *Dinamika Morskikh Voln* (Dynamics of Sea Waves) (Moscow: Izd. Moscow State University, 1985)

9. Romanov N P, Shuklin V S *Opt. Spektrosk.* **37** 1120 (1975)
10. Fadeev V V, Glushkov S M, Klimov D V, et al. *Proc. III Thematic Conf. on Remote Sensing of Marine and Coastal Environments* (Seattle, Washington, USA, 1995) vol. 2, p. 761
11. Klyshko D N, Fadeev V V *Dokl. Akad. Nauk SSSR* **238** 320 (1978)
12. Fadeev V V, Bunin D K, Venediktov P S *Kvantovaya Elektron.* **23** 963 (1996) [*Quantum Electron.* **26** 939 (1996)]
13. Filippova E M, Chubarov V V, Fadeev V V *Can. J. Appl. Spectrosc.* **38** (15) 139 (1993)
14. Fadeev V V, Dolenko T A, Filippova E M, Chubarov V V *Opt. Commun.* **166** 25 (1999)